J. Electron Microsc., Vol. 33, No. 2, 101-115, 1984

Applications of Electron Holography Using a Field-Emission Electron Microscope

Akira TONOMURA

Central Research Laboratory, Hitachi Ltd., Kokubunji, Tokyo, 185 Japan

(Received June 16, 1984; accepted June 27, 1984)

The new technique of electron holography which has recently been put to practical use with a field-emission electron microscope is reviewed. Electron holography enables discernment of the electron phase, an aspect which has not been fully utilized so far in electron microscopy. Among several applications of electron holography, interference microscopy in particular was proven to be promising for practical purposes, since the contour fringes of the transmitted electron wavefront indicated the thickness contours of a homogeneous specimen and the magnetic lines of force of a ferromagnetic specimen. Further developments of electron holography technique are expected to open new possibilities of both observation and measurements in atomic dimensions.

***Key words*=electron holography: transmission electron microscopy (TEM): field emission: interference microscopy: magnetic domain structure**

INTRODUCTION

Rapid progress in industrial technology has made it possible to control even atomic configurations in producing materials for recent devices. Consequently, observation and measurements in atomic dimensions are becoming an urgent problem for such practical purposes.

Transmission electron microscopy has been used thus far as the only tool to directly observe the microscopic structure of materials, and now, even more is demanded of it for the needs mentioned above. Although recently there has been no great progress made in electron microscopy performance, further advancement can be expected, and one possibility, I believe, is the subject of this paper, electron holography.

Electron holography[1] was invented in 1948 which broke through the limits of electron microscope resolution, but it is only recently that a coherent field-emission electron microscope has been developed for practical use.

In this paper, recent results in electron holography will be discussed, and future prospects will also be touched upon. Several comprehensive reviews of electron interferometry have recently been reported,[2-8] and consequently this paper deals mainly with our own results in electron holography using a field-emission electron microscope for the purpose of determining its practical applications.

ELECTRON HOLOGRAPHY

1. *History*

Electron holography was initially an exciting idea, but the early experimental trials were practically unsuccessful, except in the case of some basic experiments.[9,10] This is because coherent beams are indispensable for holography. However, in the early days, there were no coherent sources for either electron beams or light beams. Since the advent of laser in 1960, laser holography has become a highly developed field of light optics.

It is not true to say that no efforts were made to develop electron holography. In 1968, clear images were reconstructed by the author *et al.*[11] by adopting both Fraunhofer in-line holography and a pointed electron

cathode[10] developed by Hibi. More general off-axis holography was carried out by Möllenstedt *et al.*[12] and Tomita *et al.*[13] Further investigations have since been performed extensively by Hanszen,[8] Saxon,[14,15] Munch[16] and others. Other modes of electron holography in which transmission electron microscopes are not used, have also been reported.[17-19]

In 1968, a field-emission electron gun was developed by Crewe[20] for producing an extremely fine probe and it was also expected to provide a coherent electron beam. Several attempts[16,21-23] were made to utilize a field-emission gun as a coherent source for electron microscopes. However, rapid progress was not attained immediately from the standpoint of beam coherence. The field emission was not to blame: the electron optical system could not produce the highly collimated beam required.

With our field-emission electron microscope[24] developed in 1978, 3,000 interference fringes could be observed. The interference fringes observable, which had been limited to 300 at most, were thus increased by one order of magnitude. This improvement in beam coherence greatly enhanced electron holography techniques.

2. *Electron holography*

Electron holography is a two-step imaging method. In the first stage, a scattered wave

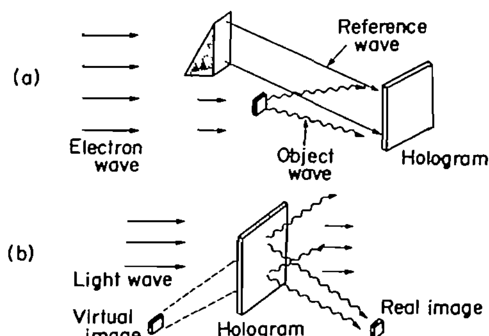

Fig. 1. Principle of electron holography. (a) Formation of electron hologram, (b) Optical image reconstruction.

from an object is recorded as an interference pattern (hologram) by projecting a reference beam onto it (Fig. 1(a)). This hologram contains all the information of the scattered electron wave, i.e. both the intensity and phase of the electron wave. Therefore, when a collimated laser beam illuminates the hologram, the original wavefront is reproduced in one of the two diffracted beams, which appear on either side of the transmitted beam. Although the wavelengths of light and electrons are quite different, the reconstructed wavefront is similar to the electron wavefront, except for some dimensions which depend on the ratio of the two wavelengths.

The reconstructed image is always accompanied by an additional image, called a conjugate image, in the other diffracted beam. This image was once considered to be a nuisance, but is now used in interference microscopy. The amplitudes of the two images are complex conjugates of each other. That is, the original wavefront is to its conjugate what an object is to its image in a mirror. Thus, once an electron wavefront is transformed completely into an optical one on an optical bench, versatile optical techniques can be applied to it.

Although only off-axis holography is explained in the illustration (Fig. 1), there is another in-line holography technique in which the direction of a reference beam is the same as that of the object beam. Furthermore, off-axis holography is classified into several types according to the optical conditions of hologram formation: Fraunhofer-,[11] Fourier-transform-[25] and image-holography,[26] in addition to the Fresnel-holography which is illustrated in Fig. 1. Although all types have already been verified to be possible for electron holography, mainly off-axis image holography will be discussed in this paper.

3. *Electron wave optics*

By means of electron holography, electron phase information can be easily observed. It will be discussed here just what kind of

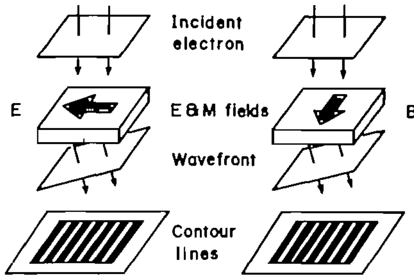

Fig. 2. Influence of electromagnetic fields on electron wavefronts. (a) Electric field, (b) Magnetic field.

information is stored in the electron phase.

Stating the conclusion first, it is electromagnetic fields, or strictly speaking, electromagnetic potentials that can be observed. This is because electrons have electric charges, through which electromagnetic fields have a physical influence on electrons. All this information is stored in the electron phase.

First, the problem will be treated semiclassically. The simplest example is illustrated in Fig. 2. Incident electrons are deflected by a uniform electric or magnetic field. When electrons are regarded as waves, it is convenient to introduce the concept of wavefront. Since the wavefront is perpendicular to rays in light optics, the relation is assumed to also hold in electron optics. Incident parallel electrons correspond to a plane wave and the deflected electrons to an inclined plane wave.

What kind of influences do electromagnetic fields have on electron wavefronts? An electric or magnetic field rotates the incident wavefront along the rotation axis determined by equipotential line or magnetic line of force, respectively. Therefore, the contour lines of the transmitted wavefront follow the equipotential lines or magnetic lines of force. This is because the height of the wavefront is always the same along the rotation axis.

Thus, the very simple conclusion could be made that the contour fringes in interference micrographs represent equipotential lines or magnetic lines of force, as viewed from the direction of the electron beam. Especially in the magnetic case, it can be concluded from the simple calculation that a constant magnetic flux of h/e (4.1×10^{-15} Wb) flows between two adjacent contour lines.

The above way of thinking is very easy to understand intuitively, but not exactly. There is an experiment called the Aharonov-Bohm effect[27] which can never be interpreted in this way. The exact treatment should start from the Schrödinger equation,

$$\left\{\frac{1}{2m}\left(\frac{\hbar}{i}\nabla+eA\right)^2-e\phi\right\}\psi=E\psi \qquad (1)$$

where m, e, ψ, E, $\hbar$, A, ϕ are the electron mass, charge, wave-function, energy, Planck's constant, vector potential and scalor potential, respectively. In the next step, the electron phase is derived from this equation.

If electromagentic fields are weak enough to modulate an incident electron beam only slightly, a solution can easily be derived using the WKB approximation. The wavefunction can be expressed by the amplitude $R(\boldsymbol{r})$ and phase $S(\boldsymbol{r})$, such that $\psi(\boldsymbol{r})=R(\boldsymbol{r})\cdot\exp(iS(\boldsymbol{r})/h)$. Equations for $R(\boldsymbol{r})$ and $S(\boldsymbol{r})$ follow

$$(\text{grad } S+eA)^2-2me\phi=\Delta R/\hbar^2R \qquad (2)$$

$$\text{div}\,(R^2\,(\text{grad } S+eA))=0 \qquad (3)$$

If the approximation, $\Delta R/\hbar^2R\ll 2me\phi$, holds, then, Eq. (2) gives

$$m\boldsymbol{v}=\text{grad } S+eA\,, \qquad (4)$$

where $\boldsymbol{v}$ is electron velocity. The meaning of this equation is easy to understand in a purely electrostatic case, where A can be made to be zero: the wavefront, i.e. the equi-phase surface is perpendicular to the electron momentum. The existence of magnetic fields, however, makes the circumstances a little complicated. That is, the wavefront is perpendicular, not to the electron momentum, $m\boldsymbol{v}$, but to the generalized momentum, $m\boldsymbol{v}-eA$.

This leads to the strange conclusion that the electron wavefront cannot be definitely defined due to the arbitrary nature of the vector potential, A, when a magnetic field exists. No counterpart to this phenomenon can be

found in light optics.

The phase can be calculated using the following equation, if the electron trajectory and potentials are known.[28]

$$S(\boldsymbol{r})=\int \mathrm{grad}\, S\cdot \boldsymbol{t}\,\mathrm{d}s$$
$$=\sqrt{2me\phi_0}\int\left(\sqrt{\frac{\phi}{\phi_0}}-\sqrt{\frac{e}{2m\phi_0}}\boldsymbol{t}\cdot\boldsymbol{A}\right)\mathrm{d}s$$
$$=p_0\int n(\boldsymbol{r},\boldsymbol{t})\mathrm{d}s\,, \tag{5}$$
$$n(\boldsymbol{r},\boldsymbol{t})=\sqrt{\frac{\phi}{\phi_0}}-\sqrt{\frac{e}{2m\phi_0}}\boldsymbol{t}\cdot\boldsymbol{A}\,, \tag{6}$$

where the integral is carried out along an electron trajectory. ϕ_0, p_0, $\boldsymbol{t}$, s and $n(\boldsymbol{r}, \boldsymbol{t})$ are the initial electron potential, momentum, unit vector of the electron trajectory, a curved coordinate along the trajectory, and the refractive index, respectively.

An electron beam passed through electromagnetic potentials contains information on those potentials, that can be expressed in the form of phase distribution. The phase distribution can be directly observed by interference microscopy, whereby electron holography is used in the manner described in the following section.

EXPERIMENTAL APPARATUS

1. Apparatus for forming electron holograms—Field emission electron microscope

Electron holograms were formed in a 125 kV field-emission electron microscope.[24] A cross-section of the apparatus is shown in Fig. 3. This microscope differs from a conventional electron microscope in two regards. One is a field-emission electron gun to provide a coherent electron beam and the other is a Möllenstedt-type electron biprism[29] as a wavefront beam splitter for forming holograms.

Details of the field-emission electron gun are illustrated in Fig. 4. Electrons are emitted from a ⟨310⟩-oriented tungsten tip, which is subjected to an ambient pressure of 10^{-10} Torr. The total emission current of 100 μm is obtained by applying an electric potential of $3\sim5$ kV between the tip and the first anode. The electrons passing through the first anode aperture are accelerated through a three-stage acceleration tube to 125 kV.

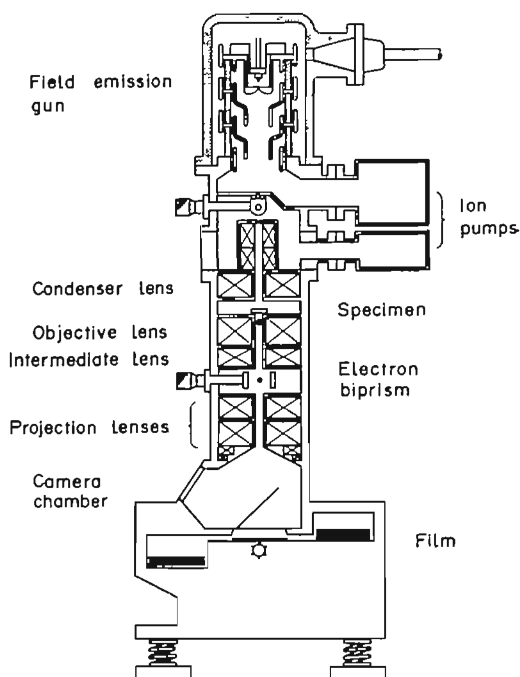

Fig. 3. Cross-section of 125 kV field-emission electron microscope.

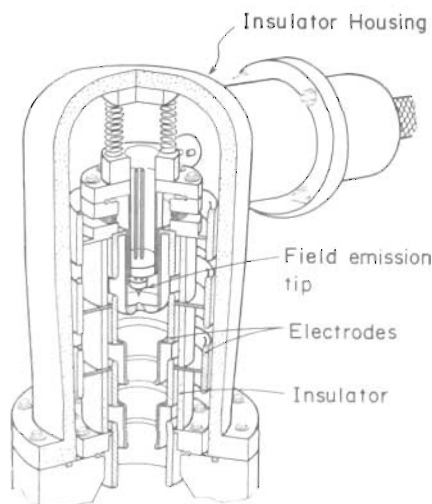

Fig. 4. Construction of field-emission electron gun.

Electrons emitted radially from the tip are

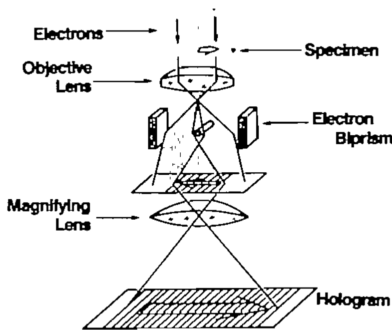

Fig. 5. Schematic diagram for electron hologram formation.

subjected to a convergent lens action near the first anode aperture and run parallel through the acceleration tube. When the accelerated electrons are focused by a single magnetic condenser lens onto a specimen plane, the diameter of the electron probe becomes approximately 300Å.

To form an electron hologram, the electron beam is overfocused to obtain a collimated beam having a divergent angle of 1×10^{-7} rad. A specimen is located in one half of the specimen plane, as shown in Fig. 5. The other half is for a reference beam. An image of the specimen is formed through an objective lens. A Möllenstedt-type electron biprism is situated between the objective lens and the image plane and is composed of a central thin wire and two ground-potential eletrodes on both sides. Application of a positive electric potential up to 200 V to the wire makes the image and the reference beam overlap. This interference pattern is magnified by enlarging lenses in the electron microscope, and is recorded on film as an electron hologram.

Not all kinds of electron holograms can be formed in the electron optical system shown in Fig. 5. The magnification is limited to $\times$ 1,000 to $\times$ 200,000. In the case of hologram formation with the magnification as low as a few thousand times, the biprism position has to be changed to between the intermediate lens and the enlarging lenses, as shown in Fig. 6. A virtual image of the specimen is formed

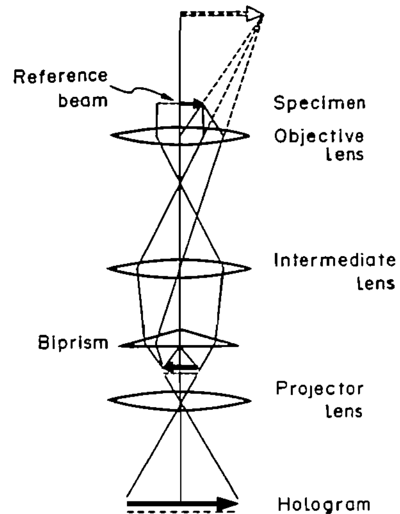

Fig. 6. Schematic diagram for electron hologram formation—In case of low magnification.

through the objective lens and then the demagnified real image is formed just below the biprism by an intermediate lens. The interference pattern formed by the biprism is magnified by the enlarging lenses. The magnification ranges from $\times$ 1,000 to $\times$ 40,000 with this electron optical system.

2. Optical reconstruction system

When a laser beam illuminates an electron hologram, the electron wavefronts are reconstructed in diffracted beams with a laser beam. Since the optical system for each purpose is different, they will be discussed separately.

1) Spherical-aberration correction[80]

The original objective of holography was to break through the resolution boundaries of the electron microscope as limited by the spherical aberration of the objective lens in the electron microscope. The situation remains true now, and, in actuality, electron micrographs of high magnification are greatly distorted by the aberration. The wavefront optically reconstructed through electron holography is also disturbed by the aberration, especially in case of a magnification higher than $\times$ 100,000. Since spherical aberration

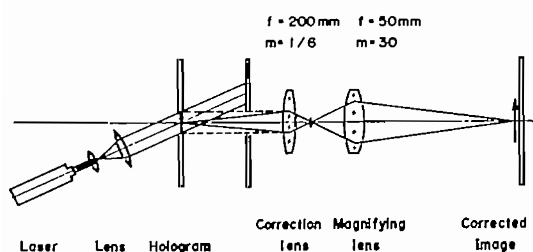

Fig. 7. Optical reconstruction system for spherical-aberration correction.

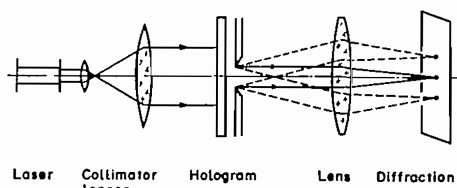

Fig. 8. Optical reconstruction system for micro-area diffraction.

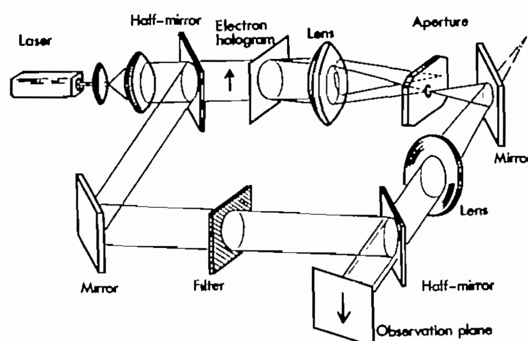

Fig. 9. Optical reconstruction system for interference microscopy.

in an electron lens is the same as that in an optical lens, except in actual dimensions, the aberrated wavefront can be optically compensated for by using the aberration of an optical lens. It is quite usual in an optical case that a spherical aberration in an optical lens system is compensated for by the combination of a concave and a convex lens.

The optical reconstruction system for aberration compensation is illustrated in Fig. 7. The reconstructed image from an electron hologram is subjected to spherical aberration C_s (C_s: spherical aberration constant in the electron microscope). However, the conjugate image, whose amplitude is a complex conjugate of the original one, is subjected to spherical aberration of $-C_s$. Therefore, the negative aberration of the conjugate image is compensated for with the positive aberration of an optical convex lens. Image demagnification is required to correspond to the large aberration of the electron lens.

2) Micro-area electron diffraction[31]

Since an electron hologram contains all the information of the transmitted electron beam, the electron diffraction pattern can be optically obtained in the reconstruction stage of electron holography. This technique has the following distinctive features compared with the conventional method used in electron microscopy.

(1) The area to be investigated can be selected in the desired shape, which is difficult with electron microscopes.

(2) Neither contamination nor radiation damage is produced during examination once a hologram is obtained.

The optical reconstruction system for electron diffraction is shown in Fig. 8. An electron hologram is illuminated by a collimated laser beam and a reconstructed image is formed in the hologram plane. The image area is selected by a field-limiting aperture also situated in the same plane. At the back focal plane of an image-forming lens, the electron diffraction pattern can be observed near the first-order diffracted spots, and the optical diffraction pattern of the electron micrograph near the primary spot.

3) Interference electron microscopy[32]

In an optically reconstructed image, the phase of the transmitted electron beam is also reconstructed. Consequently, if a plane wave overlaps the image, an interference micrograph can be obtained in which the contour lines of the transmitted wavefront are observed on an in-focus electron micrograph.

A diagram of the optical reconstruction system for interference electron microscopy is shown in Fig. 9. A collimated laser beam

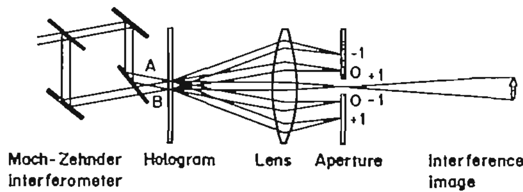

Fig. 10. Optical reconstruction system for interference microscopy—In case of phase-difference amplification.

is split into two by a half mirror. One beam illuminates an electron hologram and produces reconstructed images. One of the two images is selected by an aperture and is formed again on the observation plane by two lenses which form an afocal system. The other beam from the half mirror is sent to the observation plane as a comparison beam, forming the interference image.

There are some cases where the electron phase change in a specimen is too small to observe even a single contour fringe in its image. However, there is a way to overcome this difficulty. The method used is phase-difference amplification,[33,34] which makes good use of a conjugate image. The optical system involved is shown in Fig. 10. A collimated laser beam is split by a Mach-Zehnder interferometer into two beams travelling in different directions. These beams, A and B, illuminate the hologram, each producing three beams: a transmitted beam and two diffracted beams. In the diffracted beams, reconstructed and conjugate images appear.

A two-times phase-difference amplified interference micrograph is obtained when the reconstructed image of beam A and the conjugate image of beam B are selected by aperture and overlap to interfere with each other. This is because the wavefronts of the two reconstructed images face in opposite directions. More exactly, they are mirror-symmetrical and, therefore, the contour mapping is doubly amplified compared with the interference between a plane wave and the reconstructed image.

If higher-order diffracted beams are used, it is possible to amplify more than two times.

APPLICATIONS

1. Spherical-aberration correction of gold fine particle images[30]

The effect of the spherical aberration of the electron lens can often be recognized when crystalline specimens are observed in an electron microscope: the image formed with Bragg-reflected electrons does not coincide with an in-focus image formed with the transmitted electrons. An example of a gold fine particle is shown in Fig. 11. The Bragg-reflected beams in the specimen pass through the peripheral part of the objective lens, and are focused earlier before arriving at the

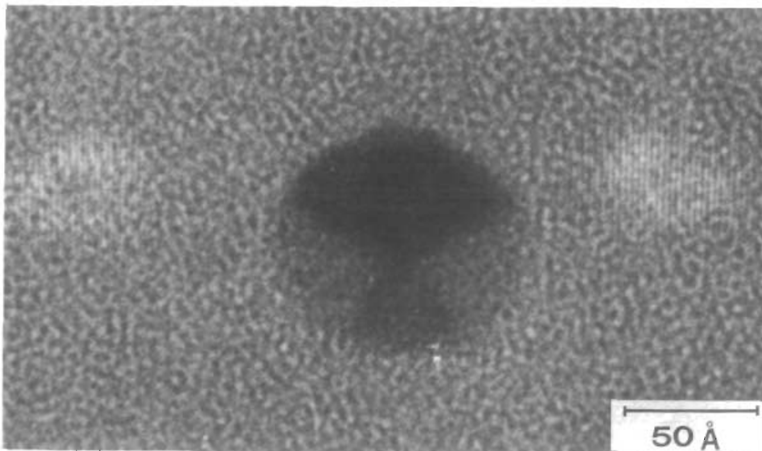

Fig. 11. In-focus electron micrograph of a gold fine particle.

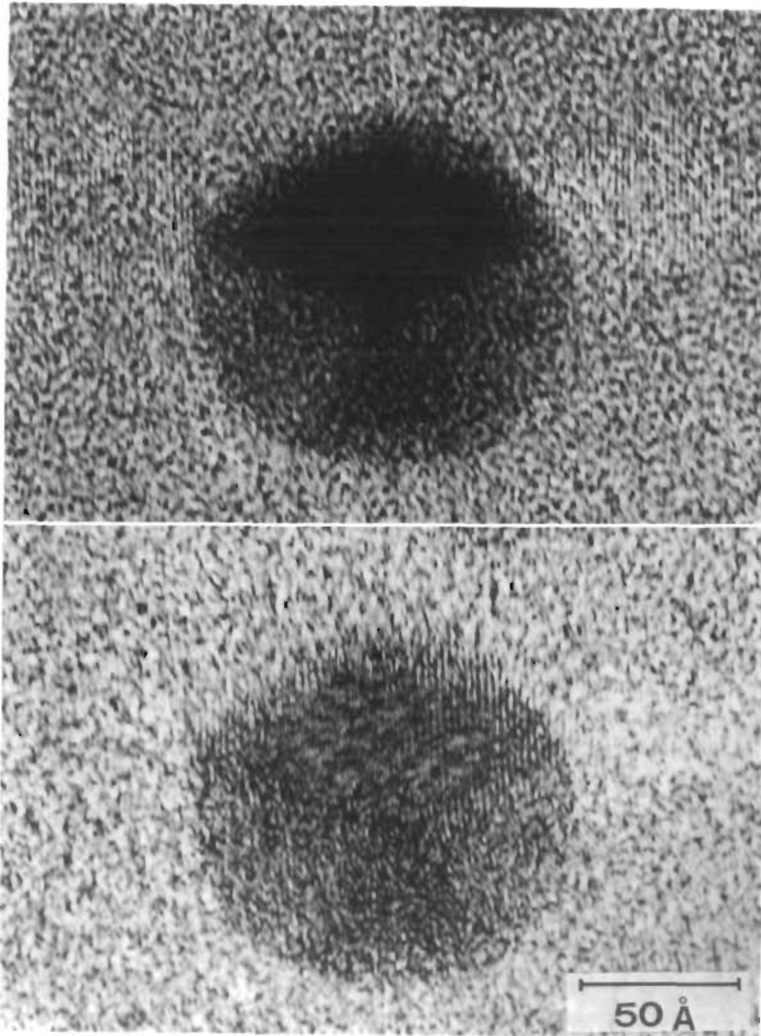

Fig. 12. Optical reconstruction of a gold fine particle. (a) Reconstructed image, (b) Spherically corrected image.

Gaussian image plane, due to the spherical aberration of the objective lens. Consequently, the two images with the reflected beams are formed at different positions from the transmitted image under the conditions of exact focusing. The interference fringes are observed inside these two reflected images, but do not indicate the existence of a crystal lattice there.

The spherically corrected image of the particle obtained using the reconstruction system in Fig. 7, is shown in Fig. 12. The reconstructed image (a) is equivalent to the electron micrograph. In the spherically corrected image (b), the two reflected images are brought to the original position, and lattice fringes are observed inside the transmitted image. The lattice fringes of the gold {111} planes (2.4Å) and also the half spacing fringes (1.2Å) are reconstructed.

Although the resolution of the reconstructed image should be better than that of the original electron micrograph, the image quality appears worse due to the backgound speckle noise. The grain size of the speckle noise can be reduced to small enough dimensions when

the spacing of the hologram carrier fringes is made smaller than the required resolution by one order of magnitude, perhaps with an electron beam with higher brightness than the present value.

2. *Low-angle electron diffraction from micro-area*[31]

Micro-area electron diffractions of a specimen can be obtained optically from the hologram whenever desired. An example of a triangular cobalt fine particle is shown in Fig. 13. Low-angle electron diffraction patterns from various micro-areas in the particle are shown. No information can be obtained from the electron micrograph (a) except the outer shape. The low-angle electron diffraction from the whole particle consists of three streaks and a central triangle. The three streaks can be shown to come from the corresponding peripheral regions A, B and C by micro-area diffraction shown in Fig. 13(e). The peripheral regions are interpreted to be wedge-shaped like prisms and deflect the electron beam in three dimensions.

It can also be concluded from Fig. 13(f), that the central triangular structure arises from the central triangular region. Since the thickness is uniform in that region, the structure is due to the magnetic domain structure in the particle. Electron diffraction patterns from various areas are obtained as shown in Fig. 13(f) in order to investigate the domain structure. The radii of the selected areas designated E (E′), F, G are 200, 150, 100Å, respectively.

A diffraction pattern from area D consists

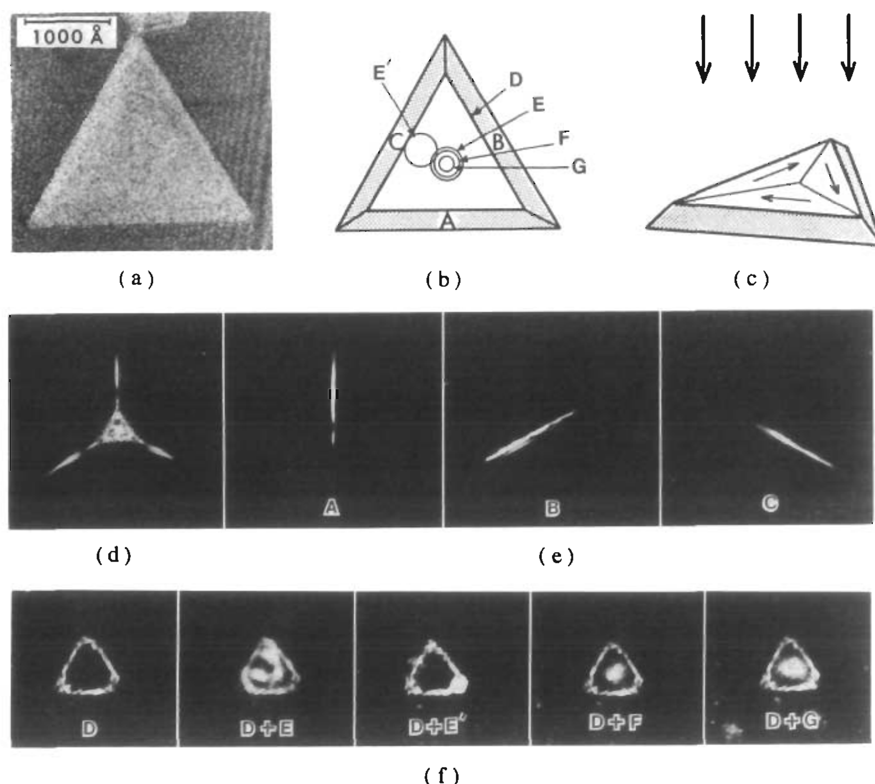

Fig. 13. Micro-area electron diffraction patterns from various regions in a cobalt particle. (a) Reconstructed image, (b) Selected areas, (c) Magnetic domain structure, (d) Diffraction pattern from the particle, (e) Diffraction patterns from peripheral regions, (f) Diffraction patterns from central regions.

of three spots and the streaks connecting them: each spot corresponds to one of the three domains. When the selected area becomes smaller, as area E, the triangle becomes smaller, but three spots are still recognized. This means that the in-plane magnetization components become smaller. Diffraction patterns from the smaller central areas F and G, are composed of only one spot. If the area E is moved to one of the three domains, a single spot appears at the vertex of the triangle.

These photographs indicate that magnetization rotates inside the particle and stands up in the central region of 150Å radius.

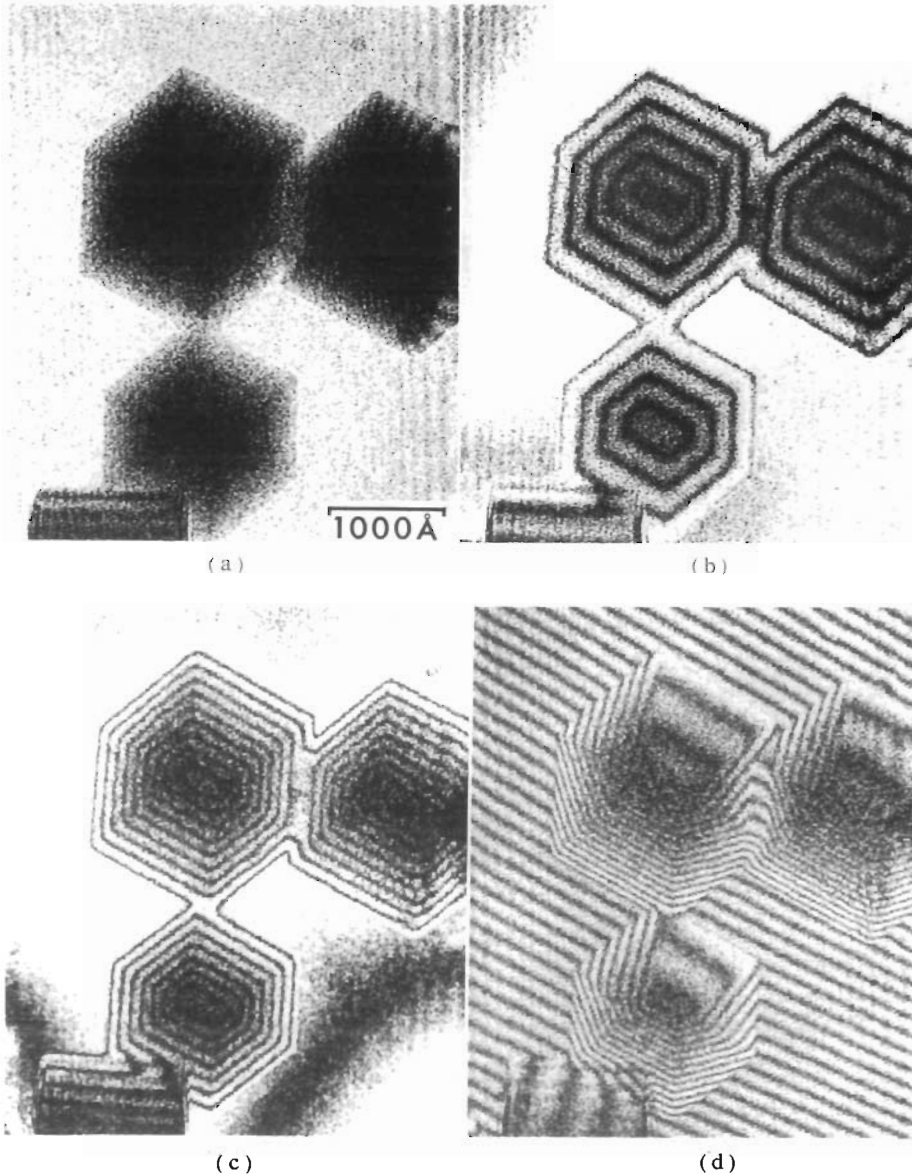

Fig. 14. Interference micrographs of MgO particles. (a) Reconstructed image, (b) Contour map, (c) Contour map ($\times 2$), (d) Interferogram ($\times 2$).

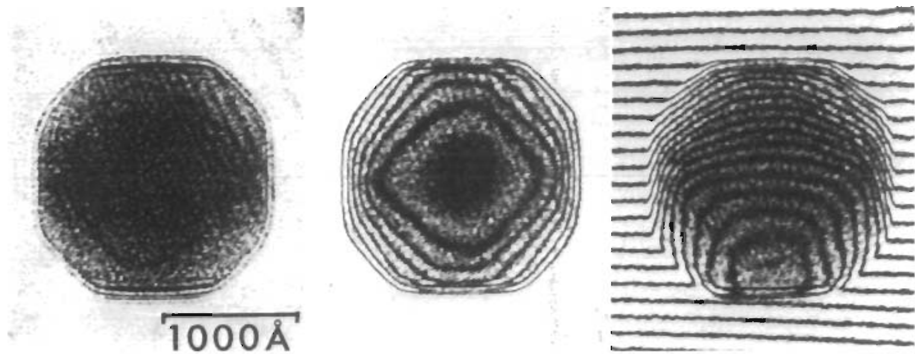

Fig. 15. Interference micrographs of a Be particle. (a) Reconstructed image, (b) Contour map (×2), (c) Interferogram (×2).

3. Thickness distribution measurement of uniform specimens

Interference electron microscopy provides information on the thickness distribution of a uniform specimen, as is the case for optical microscopy. The refractive index, n, of a nonmagnetic specimen can be derived from Eq. (6) as

$$n(\boldsymbol{r})=\sqrt{\frac{\phi_0+V_0}{\phi_0}}=1+\frac{V_0}{2\phi_0}, \qquad (7)$$

where V_0 is the inner potential of the specimen. This means that when an electron beam is passing through a specimen it is accelerated by V_0, and consequently its wavelength becomes a little shorter.

The value of V_0 is characteristic for each specific substance, and ranges from 10 to 30 volts. The second term in the refractive index is $1\sim3\times10^{-4}$ in the case of an 80-kV electron accelerating voltage. Consequently, the thickness corresponding to one wavelength shift is 150∼400Å.

Examples of interference micrographs are shown in Fig. 14. The specimen consists of MgO smoke particles. The spacing between two contour lines in Fig. 14(b) correspond to 500Å in thickness. The phase distribution is amplified two times in Fig. 14(c) and (d). The interferogram in Fig. 14(d) is obtained by changing the directions of the incident laser beams in the reconstruction stage in Fig. 10, and there the phase distribution is represented as shifts in the reference system of the regular fringes.

A beryllium particle of more complicated shape was observed by this method, as shown in Fig. 15. One-fringe spacing corresponds to 220Å, since the interference images are doubly phase-amplified. This kind of interference micrograph makes it much easier to identify the external form of a particle.

Some other interesting studies have to be mentioned here, despite using not electron holography but electron interferometry. One is concerned with the measurement of surface topology using an electron mirror interferometer, which method was developed by Lichte.[35] Surface height variations were actually measured with the precision of the order of 1Å. Another is the measurement of electric potential distributions, which possibility can easily be deduced from Eq. (7). Merli *et al.*[36] and Kuluapin *et al.*[37] investigated microelectric fields near *p-n* junctions and field-emission tips, respectively.

4. Observation of microscopic magnetic fields[38]

Interference microscopy also provides information on domain structures in a thin ferromagnetic film.* This has no counterpart in light optics. The method has the following distinctive features which have never been

* The fact that a ferromagnetic thin film presents a phase object to an illuminating electrom beam has already been confirmed from both theoretical[39-42] and experimental[43,44] aspects.

possible to achieve by any other method:[46]

(1) Microscopic magnetic lines of force can be observed as contour lines overlapping an in-focus electron micrograph.

(2) Magnetic flux can be quantitatively measured in h/e units, since a constant flux of h/e flows between two contour lines.

An example of a cobalt fine particle, which has already been used for micro-diffraction in Fig. 13, is shown in Fig. 16. No contrast is observed inside reconstructed image (a), but many contour lines appear in interference image (b). Contour lines parallel to the three edges show that the thickness increases linearly up to 550Å. The inner contour fringes are magnetic lines of force because the inner region is uniform in thickness. They clearly show how the magnetization rotates in such a fine particle.

This contour map cannot help in clarifying whether the magnetization is clockwise or counter-clockwise. The direction can be decided from interferogram (c), obtained by tilting the comparison beam in the reconstruction stage. The magnetization direction

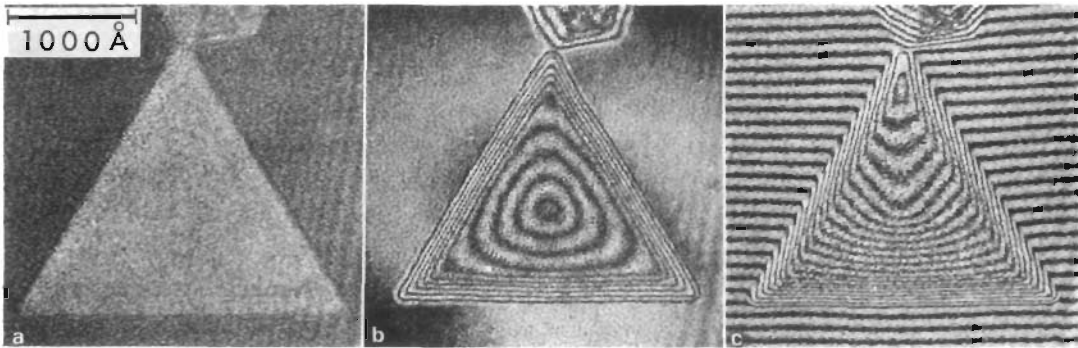

Fig. 16. Interference micrographs of a Co particle. (a) Reconstructed image, (b) Contour map (×2), (c) Interferogram (×2).

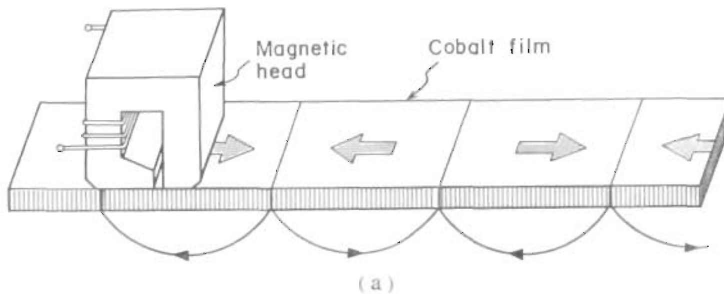

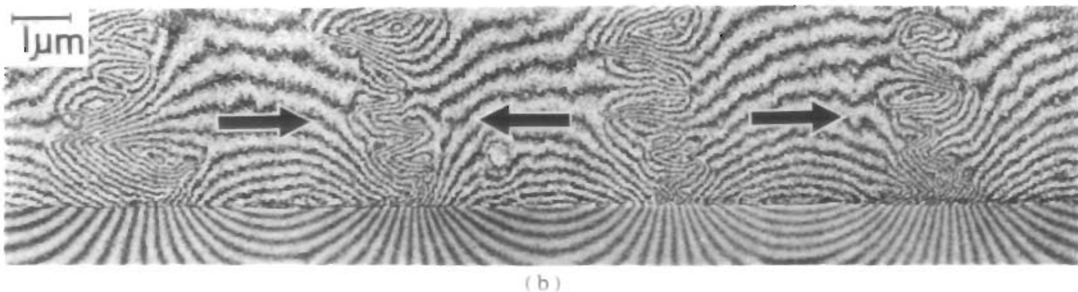

Fig. 17. Interference micrograph of magnetically-recorded Co thin film. (a) Method of magnetic recording, (b) Contour map.

proves to be counter-clockwise, since the wavefront is retarded in the center on the particle.

Another example is shown in Fig. 17.[46,47] The specimen is a thin cobalt film on which magnetic recording was carried out with a moving magnetic head. The film is observed from above. Recorded magnetization inside the film, the direction of which is indicated by arrows, can be observed as well as the magnetic fields leaking from it. Two oppositely directed streams of magnetization collide head on, and produce vortices similar to the way in which streams of water do.

Such observation of detailed magnetic field distribution is very helpful for the study of high density magnetic recording. In actuality, the suitability of recording with a 0.15 μm unit length has been confirmed with the help of this method.

5. Experiment on the Aharonov-Bohm effect

An electron beam interacts directly with electromagnetic potentials rather than with electromagnetic fields, as was mentioned before. This can also be inferred from the fact that both the Shrödinger Eq. (1) and refractive index (6) are represented by electromagnetic potentials. This can be ingeneously shown by an experiment that has been theoretically proposed by Aharonov and Bohm. The experiment is shown schematically in Fig. 18. In their proposal, two electron beams from a single point pass on both sides of an infinitely long solenoid, and are superimposed with a biprism to form an interference pattern. When an electric current is applied to produce a magnetic field inside the solenoid, an additional phase shift will be produced between the two beams, even though the magnetic fields remain at zero along the two paths. Vector potentials are the cause of this phenomenon.

This Aharonov-Bohm (AB) effect was confirmed by several technically sophisticated experiments.[48-51] The significance of the AB effect was not, however, fully recognized until recently, when the theory of gauge fields was rediscovered as a basic principle of physics. A vector potential is an example of a gauge field, and the AB effect is regarded by Wu and Yang[52] as only an experimental manifestation of gauge theory in the area of electromagnetism.

Recently, controversy has flared up concerning the existence of this effect. Bocchieri and Loinger[53] assert that the AB effect does not exist, and that it is of purely mathematical origin. The previously mentioned experiments, they say, do not confirm the effect because of inevitable leakage flux from the finite whiskers or solenoids used in these experiments.

To help clarify things, a new experiment was carried out to remove any vagueness regarding leakage effects using the electron holography technique.[54-56] Tiny toroidal magnets were fabricated by electron beam lithog-

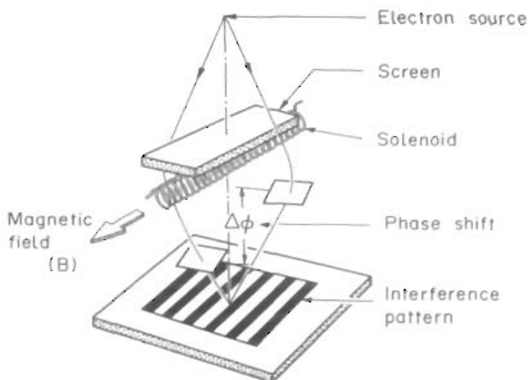

Fig. 18. Experiment involving Aharonov-Bohm effect.

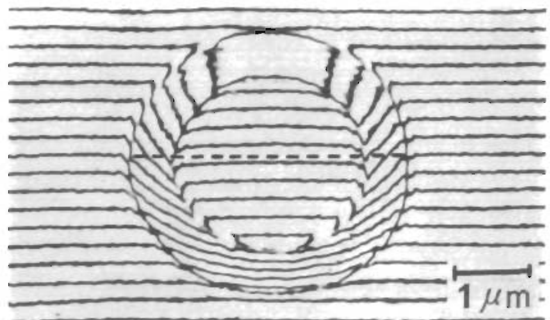

Fig. 19. Interferogram of a toroidal ferromagnet.

raphy. Magnetic flux was completely within the magnets, and the amount of the leakage flux as measured by interference microscopy was confirmed to be too small to cause an imaginary AB effect.

The interference pattern between the electron beam transmitted through a toroidal magnet, and a slightly tilted reference beam is shown in Fig. 19. This photograph reveals that a phase difference really exists between the electron beam that passes through the hole of the magnet and the beam passing outside the magnet, where there is no magnetic field. This result supports the fact that vector potential is a physical entity, and consequently confirms the existence of the AB effect.

FUTURE PROSPECTS

Phase information has played an invaluable role in both image observation and measurements in light optics. However, it has scarcely been utilized in electron microscopy, though an electron beam provides possibilities of measurements in atomic dimensions, making the best use of short wavelengths of far less than 1Å. The reason why this has not been realized, is that there are neither coherent sources nor versatile optical parts in electron optics.

The situation has improved a little since the utilization of a field-emission electron beam as a coherent electron beam. But the situation of having no optical parts available remains the same. Here, electron holography enters the stage. Once an electron hologram is recorded, the electron wavefronts are reproduced as optical ones. Since the stage is an optical bench, numerous possibilities are opened up using optical techniques.

Up to now, it has become possible to detect phase change of an electron beam down to $1/10\lambda$. If the detection limit further improves by one order of magnitude, the world of electron microscopy will be brought to life again by the introduction of the electron phase.

REFERENCES

1) Gabor, D.: *Proc. R. Soc.*, A **197**, 454 (1949)
2) Hibi, T. and Yada, K.: Principles and Techniques of Electron Microscopy, van Nostrand, Amsterdam, 1976, Vol. 6, p. 312
3) Hawkes, P. W.: Advances in Optical and Electron Microscopy, Academic Press, London, 1978, Vol. 7, p. 101
4) Zeitler, E.: Proc. 37th EMSA Meeting, Claitor, Baton Rouge, 1979, p. 376
5) Rogers, J.: Imaging Processes and Coherence in Physics, Springer Verlag, Berlin, 1980, p. 365
6) Wade, R. H.: Computer Processing of Electron Microscope Images, Springer Verlag, Berlin, 1980, p. 223
7) Missiroli, G. F., Pozzi, G. and Valdrè, U.: *J. Phys.* E, **14**, 649 (1981)
8) Hanszen, K.-J.: Advances in Electronics and Electron Physics, Academic Press, New York, 1982, Vol. 59, p. 1
9) Haine, M. E. and Mulvey, T.: *J. Opt. Soc. Am.*, **42**, 763 (1952)
10) Hibi, T.: *J. Electron Microsc.*, **4**, 10 (1956).
11) Tonomura, A., Fukuhara, A., Watanabe, H., and Komoda, T.: *Jpn. J. Appl. Phys.*, **7**, 226 (1968)
12) Möllenstedt, G. and Wahl, H.: *Naturwissenschaft*, **55**, 340 (1968)
13) Tomita, H., Matsuda, T. and Komoda, T.: *Jpn. J. Appl. Phys.*, **11**, 143 (1972)
14) Saxon, G.: *Optik*, **35**, 195 (1972)
15) Saxon, G.: *Optik*, **35**, 359 (1972)
16) Munch, J.: *Optik*, **43**, 79 (1975)
17) Stroke, G. W. and Halioua, M.: *Optik*, **35**, 50 (1972)
18) Veneklasen, L. H.: *Optik*, **44**, 447 (1975)
19) Bartell, L. S.: *Optik*, **43**, 373 (1975)
20) Crewe, A. V., Eggenberger, D. N., Wall, D. N. and Welter, L. N.: *Rev. Sci. Instrum.*, **39**, 576 (1968)
21) Tonomura, A. and Komoda T.: *J. Electron Microsc.*, **22**, 141 (1973)
22) Someya, T., Goto, T., Harada, Y., Yamada, K., Koike, H., Kokubo, Y. and Watanabe, M.: *Optik*, **41**, 225 (1974)
23) Troyon, M.: *Optik*, **46**, 439 (1976)
24) Tonomura, A., Matsuda, T., Endo, J., Todokoro, H. and Komoda, T.: *J. Electron Microsc.*, **28**, 1 (1979)
25) Lauer, R.: *Optik*, **66**, 159 (1984)
26) Weingärtner, I., Mirandé, W. and Menzel, E.: *Optik*, **30**, 318 (1969)
27) Aharonov, Y. and Bohm, D.: *Phys. Rev.*, **115**, 485 (1959)

28) Ehrenberg, W. and Siday, R. E.: *Proc. Phys. Soc. London*, B **62**, 8 (1949)
29) Möllenstedt, G. and Dücker, H.: *Z. Phys.*, **145**, 375 (1956)
30) Tonomura, A., Matsuda, T. and Endo, J.: *Jpn. J. Appl. Phys.*, **18**, 1373 (1979)
31) Tonomura, A. and Matsuda, T.: *Jpn. J. Appl. Phys.*, **19**, L97 (1980)
32) Tonomura, A., Endo, J. and Matsuda, T.: *Optik*, **53**, 143 (1979)
33) Matsumoto, K. and Takashima, M.: *J. Opt. Soc. Am.*, **60**, 30 (1970)
34) Endo, J., Matsuda, T. and Tonomura, A.: *Jpn. J. Appl. Phys.*, **18**, 2291 (1979)
35) Lichte, H.: *Optik*, **57**, 35 (1980)
36) Merli, P. G., Missiroli, G. F. and Pozzi, G.: *J. Microsc. (Paris)*, **21**, 11 (1974)
37) Kulyupin, Yu. A., Nepijko, S. A., Sedov, N. N. and Shamonya, V. G.: *Optik*, **52**, 101 (1978/1979)
38) Tonomura, A., Matsuda, T., Endo, J., Arii, T. and Mihama, K.: *Phys. Rev. Lett.*, **44**, 1430 (1980)
39) Cohen, M. S.: *J. Appl. Phys.*, **38**, 4966 (1967)
40) Olivei, A.: *Optik*, **33**, 93 (1971)
41) Lau, B. and Pozzi, G.: *Optik*, **51**, 287 (1978)
42) Wahl, H. and Lau, B.: *Optik*, **54**, 27 (1979)
43) Tonomura, A.: *Jpn. J. Appl. Phys.*, **11**, 493 (1972)
44) Pozzi, G. and Missiroli, G. F.: *J. Microsc. (Paris)*, **18**, 103 (1973)
45) Tonomura, A., Matsuda, T., Tanabe, H., Osakabe, N., Endo, J., Fukuhara, A., Shinagawa, K. and Fujiwara, H.: *Phys. Rev.* B, **25**, 6799 (1982)
46) Osakabe, N., Yoshida, K., Horiuchi, Y., Matsuda, T., Tanabe, H., Okuwaki, T., Endo, J., Fujiwara, H. and Tonomura, A.: *Appl. Phys. Lett.*, **42**, 746 (1983)
47) Yoshida, K., Okuwaki, T., Osakabe, N., Tanabe, H., Horiuchi, Y., Matsuda, T., Shinagawa, K., Tonomura, A. and Fujiwara, H.: *IEEE Trans. Mag.*, MAG-**19**, No. 5, 1600 (1983)
48) Chambers, R. G.: *Phys. Rev. Lett.*, **5**, 3 (1960)
49) Fowler, H. A., Marton, L., Simpson, J. A. and Suddeth, J. A.: *J. Appl. Phys.*, **32**, 1153 (1961)
50) Boersch, H., Hamisch, H., Grohmann, K. and Wohlleben, D.: *Z. Phys.*, **165**, 79 (1961)
51) Möllenstedt, G. and Bayh, W.: *Phys. Bl.*, **18**, 299 (1962)
52) Wu, T. T. and Yang, C. N.: *Phys. Rev.* D, **12**, 3845 (1975)
53) Bocchieri, P. and Loinger, A.: *Nuovo Cimento*, Ser. 2, **47A**, 475 (1978)
54) Tonomura, A., Matsuda, T., Suzuki, R., Fukuhara, A., Osakabe, N., Umezaki, H., Endo, J., Shinagawa, K., Sugita, Y. and Fujiwara, H.: *Phys. Rev. Lett.*, **48**, 1443 (1982)
55) Tonomura, A., Umezaki, H., Matsuda, T., Osakabe, N., Endo, J. and Sugita, Y.: *Phys. Rev. Lett.*, **51**, 331 (1983)
56) Tonomura, A., Umezaki, H., Matsuda, T., Osakabe, N., Endo, J., and Sugita, Y.: Proc. Int. Symp. on Foundations of Quantum Mechanics, Physical Society of Japan, Tokyo, 1984, p. 20